swine antibody to rabbit IgG (diluted 1:40) was used to visualize PNSG. Cover slips were mounted with Permafluor and analyzed with a fluorescence microscope as described (9). Each sputum sample was analyzed twice.
8. D. McKenney *et. al.*, unpublished data.
9. S. Herbert *et al.*, *J. Infect. Dis.* **176**, 431 (1997).
10. J. C. Lee *et al.*, *J. Clin. Microbiol.* **28**, 2612 (1990).
11. For detection of PNSG expression by fresh clinical isolates, we used a sensitive ELISA inhibition that was slightly modified from the previously described procedure (5), as well as immunoelectron microscopy (5). Bacterial cells were suspended to an optical density at 650 nm of 2.0 in 0.1 M phosphate and 0.15 M NaCl [phosphate-buffered saline (PBS)] and then treated with trypsin (0.65 mg/ml for 30 min at 37°C) to destroy antibody-binding structures such as protein A present on the surface of most *S. aureus* strains [B. F. King and B. J. Wilkinson, *Infect. Immun.* **33**, 666 (1981)]. After washing, the bacterial pellet was suspended in a 1:500 dilution of antiserum to PNSG and incubated at 4°C overnight, after which cells were removed and adsorbed sera were tested for residual binding activity in a PNSG-specific ELISA as described (5).
12. C. Heilmann *et al.*, *Mol. Microbiol.* **20**, 1083 (1996); C. Gerke *et al.*, *J. Biol. Chem.* **273**, 18586 (1998).
13. Primers were designed to amplify a gene product of 2.7 kb encompassing a region of the *icaADBC* genes of the staphylococcal *ica* locus (12). The PCR forward primer was TGCACTCAATGAGGGAATCA, corresponding to nucleotides 409 to 428 in the *icaA* gene; the reverse primer was AATCACTACCGGAAACAGCG, complementary to nucleotides 3114 to 3133 in the *icaC* gene. PCR was carried out with Platinum PCR Supermix and 200 nM primers. DNA melting was at 95°C for 30 s, annealing was at 60°C for 60 s, and elongation was at 72°C for 60 s; repeat cycles decreased the annealing temperature by 0.5°C each cycle until 28 cycles were completed. Amplified DNA was visualized after separation in a 0.7% agarose gel and staining with ethidium bromide.
14. With the use of the blastN and blastT search programs [S. F. Altschul *et al.*, *J. Mol. Biol.* **215**, 403 (1990)] on the unfinished nucleotide sequences of the *S. aureus* NCTC 8325-4 genome (University of Oklahoma's Advanced Center for Genome Technology) and the *S. aureus* COL genome (Institute for Genome Research), there was 71 and 74% identity, respectively, with the *ica* locus of *S. epidermidis* RP62A (accession number U43366). The predicted protein sequences from *S. aureus* shared 72% identity and 80% (NCTC 8325-4) and 87% (COL) similarity to the *S. epidermidis* icaADBC proteins. The matches were on three unassembled fragments (contigs 1441, 1348, and 1147) of the NCTC 8325-4 genome sequence and in the proper order on a single fragment (gsa–76) of 9459 base pairs of the COL genome sequence. The GCG suite of programs (Wisconsin Package 9.1; Genetics Computer Group, Madison WI) was used to assemble the fragments of the *S. aureus* NCTC 8325-4 genome for translation and analysis.
15. Y. Wang and R. I. Hollingsworth, *Carbohydr. Res.* **260**, 305 (1994).
16. Swiss Webster mice were actively immunized IP with three 100-μg doses of PNSG 5 to 6 days apart or identically with a control polysaccharide antigen from *P. aeruginosa*. Five days after the last dose, the mice were challenged with *S. aureus*, and infection was allowed to proceed for 5 days, after which the mice were killed and bacterial counts on kidney homogenates were performed. The significance of the differences in CFU per gram of kidney between PNSG-immune and control mice was determined by a *t* test. All mice were treated in accordance with institutional guidelines for the humane care and treatment of animals.
17. J. C. Lee and G. B. Pier, in *The Staphylococci in Human Disease*, K. Crossley and G. L. Archer, Eds. (Churchill Livingstone, New York, 1997), pp. 631–654.
18. A. I. Fattom *et al.*, *Infect. Immun.* **64**, 1659 (1996).
19. Three examples are shown of eight tested, representative of five PNSG-negative, two PNSG-low, and one PNSG-intermediate strain at challenge. Baseline values for percentage of inhibition of antibody binding ± the standard error for *S. aureus* are as follows: strain Por = 0 ± 9%, strain 5836 = 21 ± 4%, and strain 5827 = 48 ± 5%.
20. W. R. Schwan *et al.*, *Infect Immun* **66**, 567 (1998); A. M. Lowe, D. T. Beattie, R. L. Deresiewicz, *Mol. Microbiol.* **27**, 967 (1998); J. M. Mei, F. Nourbakhsh, C. W. Ford, D. W. Holden, *ibid.* **26**, 399 (1997).
21. H. Shiro, *et al.*, *Circulation* **92**, 2715 (1995).
22. A. Fattom *et al.*, *Infect. Immun.* **61**, 1023 (1993); A. Fattom *et al.*, *ibid.* **60**, 584 (1992); J. C. Lee *et al.*, *ibid.* **65**, 4146 (1997).
23. N. Balaban *et al.*, *Science* **280**, 438 (1998).
24. W. Mamo, M. Boden, J. I. Flock, *FEMS Immunol. Med. Microbiol.* **10**, 47 (1994); T. Schennings *et al.*, *Microb. Pathog.* **15**, 227 (1993); I. M. Nilsson *et al.*, *J. Clin. Invest.* **101**, 2640 (1998).
25. E. Muller *et al.*, *J. Infect. Dis.* **168**, 1211 (1993); W. Ziebuhr *et al.*, *Infect. Immun.* **65**, 890 (1997).
26. S. Takeda *et al.*, *Circulation* **84**, 2539 (1991); Y. Kojima *et al.*, *J. Infect. Dis.* **162**, 435 (1990).
27. For characterization of PNSG production in *S. aureus*–infected lungs, bronchial tissue pieces (2 mm by 2 mm) from right upper lobes of two 8-year-old female CF patients who underwent lobectomy because of chronic *S. aureus* infection were embedded in agarose and thereafter in K11M for sectioning. Ultrathin sections (0.1 to 0.2 μm) were fixed on glass slides, and nonspecific binding of antibodies to Protein A was blocked with swine serum diluted 1:10 in PBS (pH 7.4) supplemented with 0.1% Tween 20 for 1 hour at room temperature. After washing with PBS–Tween 20, sections were incubated with rabbit antibody to *S. aureus* PNSG for 1 hour at room temperature in a wet chamber, followed by incubation with a mouse monoclonal IgG antibody to the CP5 or CP8 antigen of *S. aureus* for 1 hour, and then washed with PBS–Tween 20. For detection of PNSG expression, sections were incubated for 40 min with CY3-indocarbocyanine–conjugated antibody to rabbit IgG diluted 1:500 in PBS–Tween 20. For detection of CP antigens, sections were incubated with FITC-conjugated antibody to mouse IgG diluted 1:200 in PBS–Tween 20. After washing, DNA was stained with 1 μg of 4′,6-diamidino-2-phenylindole, dilactate (DAPI) per milliliter for 5 min, and sections were washed again with distilled water; the sections were embedded in Permafluor and analyzed with a fluorescence microscope (9).
28. PNSG was used to immunize rabbits to obtain specific antibodies. After an antibody titer >1000 was detected by ELISA, immune rabbit sera were used for protection studies in the mouse renal abscess model [A. Albus, R. D. Arbeit, J. C. Lee, *Infect. Immun.* **59**, 1008 (1991)]. Control sera were from rabbits immunized with the irrelevant *P. aeruginosa* polysaccharide. Six- to eight-week-old Swiss Webster mice were treated with 0.5 ml of rabbit serum IP 4 hours before challenge with *S. aureus* strains and again 18 hours later. Infection was allowed to proceed for 5 days, after which the mice were killed and bacteria were counted in kidney homogenates (16).
29. *Staphylococcus aureus* cells growing on primary cultures from infected mouse kidneys were scraped directly from TSA plates into PBS. A 1-ml volume of the cells was centrifuged (15,000*g*, 5 min), washed in sterile PBS, and treated with trypsin (0.65 mg/ml for 30 min at 37°C). Electron microscopic grids were prepared and processed for viewing as described (5). The grids were examined with a transmission electron microscope at magnifications of 6000 to 25,000.
30. We thank J. Hübner and E. Muller for helpful input, F. Tenover for MRSA-VISA strains, A. Onderdonk for clinical isolates, R. Ross for *S. aureus* strain MN8m, L. Almeida for assistance with colony immunoblots, A. Fattom for human antibodies to CP5 and CP8, M. Coyne for assistance with analysis of *S. aureus* genome sequences, J. M. Fournier for monoclonal antibodies to CP5 and CP8, S. Campana and L. Marianelli for supplying CF sputum samples, and G. Bellon for CF lung tissue. Supported by NIH grant AI23335.

13 January 1999; accepted 20 April 1999

Spatiotemporal Dynamics of Inositol 1,4,5-Trisphosphate That Underlies Complex Ca^{2+} Mobilization Patterns

Kenzo Hirose,* Shiro Kadowaki, Mao Tanabe, Hiroshi Takeshima, Masamitsu Iino

Inositol 1,4,5-trisphosphate (IP_3) is a second messenger that elicits complex spatiotemporal patterns of calcium ion (Ca^{2+}) mobilization and has essential roles in the regulation of many cellular functions. In Madin-Darby canine kidney epithelial cells, green fluorescent protein–tagged pleckstrin homology domain translocated from the plasma membrane to the cytoplasm in response to increased concentration of IP_3. The detection of translocation enabled monitoring of IP_3 concentration changes within single cells and revealed spatiotemporal dynamics in the concentration of IP_3 synchronous with Ca^{2+} oscillations and intracellular and intercellular IP_3 waves that accompanied Ca^{2+} waves. Such changes in IP_3 concentration may be fundamental to Ca^{2+} signaling.

IP_3 production by phospholipase C (PLC)–mediated hydrolysis of phosphatidylinositol 4,5-bisphosphate (PIP_2) is an early intracellular event after stimulation by hormones, autacoids, and neurotransmitters. IP_3 mobilizes Ca^{2+} from intracellular stores through the IP_3 receptor, resulting in activation of Ca^{2+}-dependent cellular events such as contraction, secretion, gene expression, and synaptic plasticity (*1*, *2*). Ca^{2+} mobilization occurs in complex temporal and spatial patterns, including Ca^{2+} oscil-

Department of Pharmacology, Faculty of Medicine, University of Tokyo and CREST, Japan Science and Technology Corporation, Tokyo 113-8654, Japan.

*To whom correspondence to be addressed. E-mail: hirose@calcium.cmp.m.u-tokyo.ac.jp

lations (*3*) and Ca^{2+} waves (*4*). However, the mechanism underlying the generation of the complex patterns has not been fully elucidated, partly because of lack of knowledge regarding IP_3 dynamics in single cells.

Green fluorescent protein (GFP)–based probes have been used to analyze cellular signaling because they have the advantage that they can be DNA encoded (*5*). Fusion proteins consisting of GFP and a functional protein domain can function as molecular probes when their intracellular translocation pattern can be visualized (*6*). The GFP-tagged pleckstrin homology (PH) domain of PLC-δ_1 (GFP-PHD) is one such probe because it binds to PIP_2 within the plasma membrane and translocates to the cytoplasm after receptor stimulation (*7*). Although the translocation was thought to reflect a decrease in the PIP_2 concentration (*7*), we obtained evidence that an increase in the cytoplasmic IP_3 concentration ($[IP_3]_i$) causes the translocation of GFP-PHD, and therefore we used GFP-PHD to monitor spatiotemporal changes in $[IP_3]_i$ that underlie the complex Ca^{2+} mobilization patterns within single living cells.

We analyzed PIP_2 binding of the PH domain of PLC-δ_1 (*8*) by a surface plasmon assay (*9*) and obtained dissociation constants (K_d) of 2.8 and 2.1 μM for PH

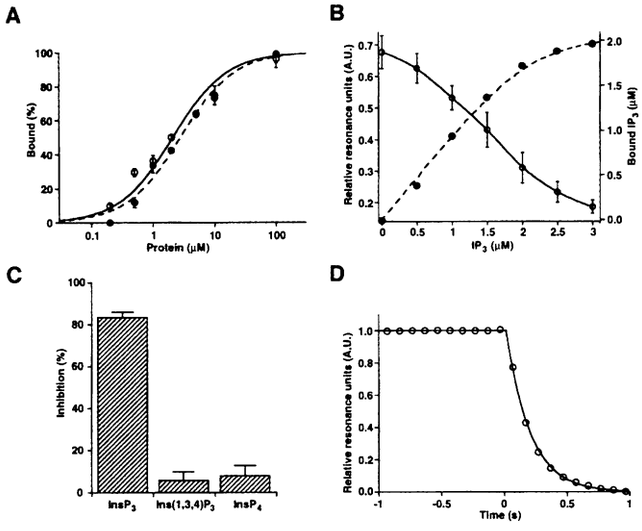

Fig. 1. In vitro characterization of GFP-PHD. (**A**) Dose dependence of the PIP_2 binding of the PH domain with (●, dashed curve) and without (○, solid curve) GFP. Average ± SEM (n = 3). (**B**) Dose-dependent inhibition (○) of PIP_2 binding of the PH domain (2 μM) and estimated IP_3 binding to the PH domain (●) (n = 3). (**C**) Inhibition of PIP_2 binding of 2 μM GFP-PHD by 2 μM IP_3 ($InsP_3$), inositol 1,3,4-trisphosphate [$Ins(1,3,4)P_3$], and inositol 1,3,4,5-tetrakisphosphate ($InsP_4$). (**D**) Dissociation of GFP-PHD from PIP_2. At time zero, GFP-PHD was removed and IP_3 (400 μM) was introduced. A.U., arbitrary units.

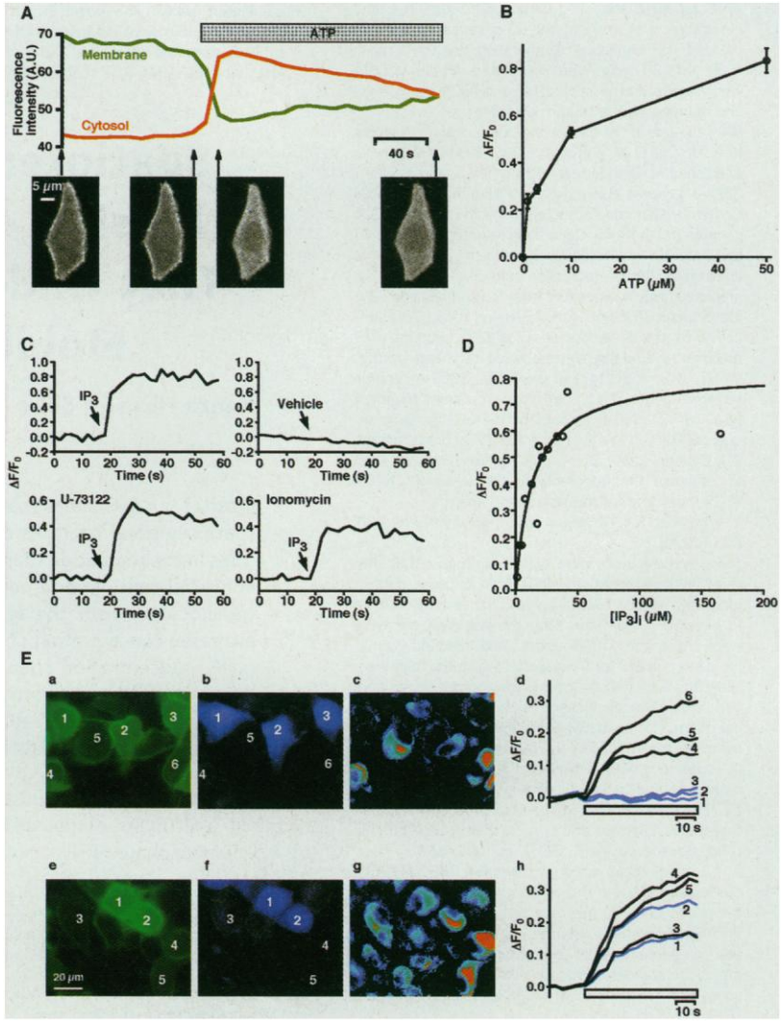

Fig. 2. Translocation of GFP-PHD induced by IP_3. (**A**) Cells challenged with 50 μM ATP were examined by confocal microscopy. Time courses of the fluorescence intensities in the membrane [defined by the bright peripheral region (widths, 1 μm) of the cells before stimulation] and cytoplasmic regions are shown together with the images at the time points indicated (arrows). Data shown are representative of four determinations. The membrane region was separately verified with a membrane probe, FM4-64. (**B**) Dependence of the extent of cytoplasmic translocation on ATP concentration. $\Delta F/F_0$, fractional changes in fluorescence intensity. (**C**) Effect of microinjection of IP_3 (final concentration, ~80 μM) or vehicle on cytoplasmic translocation of GFP-PHD in the absence of extracellular Ca^{2+}. Experiments were also performed after treatment with U73122 (5 μM) and ionomycin (10 μM). Data shown are representative of three experiments. (**D**) IP_3 dependence of GFP-PHD translocation. $[IP_3]_i$ was estimated by fluorescence of rhodamine-dextran with which IP_3 (100 to 500 μM) was coinjected. (**E**) Effect of IP_3 5-phosphatase on the translocation of GFP-PHD. GFP-PHD–expressing cells transfected with pcDNA3.1-IP_3 5-phosphatase (**a** to **d**) and pcDNA3.1-EBFP or pcDNA3.1 and pcDNA3.1-EBFP (**e** to **h**) were imaged with a CCD camera. The fluorescence images of GFP-PHD (a and e) and BFP (b and f) are shown. (c) and (g) are GFP-PHD images divided by the average of 10 consecutive images before stimulation. The time course of cytoplasmic translocation is shown (d and h). ATP (50 μM, open bar) was applied after ionomycin treatment and in the presence of a low extracellular Ca^{2+} concentration (1 μM) to avoid intracellular Ca^{2+} elevation that might secondarily augment PIP_2 hydrolysis. Similar results were obtained in cells without such treatment. Data shown are representative of four experiments.

domains with and without GFP tagging, respectively (Fig. 1A). IP_3 inhibited this binding in a dose-dependent manner, and the K_d for IP_3 was 93 nM (Fig. 1B), indicating that IP_3 binds to this PH domain with a ~20-fold higher affinity than PIP_2, consistent with previous reports (*10*). IP_3 inhibited the binding of GFP-PHD to PIP_2 (Fig. 1C) with similar efficiency, indicating no impairment of IP_3 binding by GFP tagging. Inositol 1,3,4-trisphosphate and inositol 1,3,4,5-tetrakisphosphate displaced little GFP-PHD from PIP_2 (Fig. 1C). This result confirms the ligand recognition specificity of the PH domain (*10*). The off rate (k_{off}) deduced from the dissociation curve was 5.25 s^{-1} (Fig. 1D), which indicates the lower limit of the actual k_{off} because of the limited time resolution. Thus, IP_3 rapidly displaces GFP-PHD from PIP_2 with high affinity and specificity. We, therefore, studied the movement of GFP-PHD within living cells in conjunction with the receptor-mediated phosphatidylinositol turnover.

GFP-PHD was expressed in Madin-Darby canine kidney (MDCK) epithelial cells (*11*), and localization of its fluorescence was examined under a confocal microscope (*12*). GFP-PHD was concentrated at the plasma membrane (Fig. 2A). Cells expressing GFP alone showed homogeneous cytoplasmic and nuclear staining (*13*). Thus, GFP-PHD preferentially interacts with a plasma membrane component, presumably PIP_2, as does full-length PLC-δ_1 (*14*). In cells treated with adenosine triphosphate (ATP), fluorescence intensity of GFP-PHD in the cytoplasmic region increased, whereas that at the plasma membrane decreased (Fig. 2A). Removal of ATP restored the original fluorescence distribution (*13*). Neither binding of IP_3 nor binding of PIP_2 in vitro changed the fluorescence intensity of GFP-PHD (*13*). Thus, the observed changes in the fluorescence intensity apparently reflect the translocation of GFP-PHD and were ATP concentration dependent (Fig. 2B). Similar results were observed in cells stimulated with bradykinin (*13*).

Microinjection of IP_3 induced transloca-

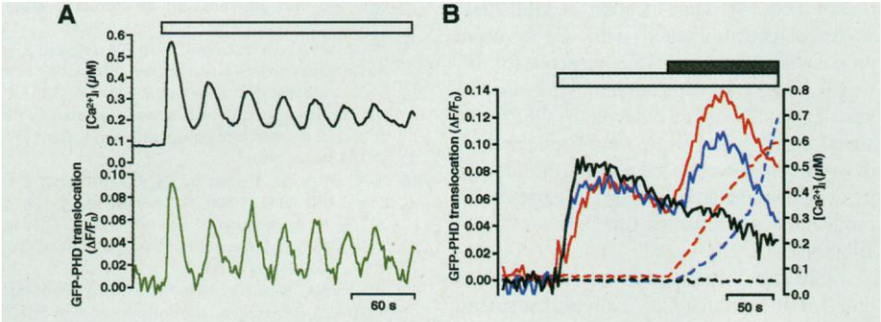

Fig. 3. Temporal dynamics of IP_3. (**A**) IP_3 oscillations (bottom traces) monitored by GFP-PHD translocation during Ca^{2+} oscillations (top traces) elicited by the application of 3 μM ATP (open bar). Representative data from at least 11 oscillating cells are shown. (**B**) Time courses of GFP-PHD translocation (solid traces) and $[Ca^{2+}]_i$ (dashed traces) during ATP (3 μM) application (open bar) and subsequent introduction of extracellular Ca^{2+} (gray bar) in the cells pretreated with ionomycin (10 μM) in the absence of Ca^{2+}. Black, blue, and red traces denote those time courses with the introduction of 0, 100, and 300 μM Ca^{2+}, respectively. (**C**) Additional increase in GFP-PHD translocation 60 s (red) or 120 s (blue) after the introduction of Ca^{2+} (0, 10, 100, and 300 μM), plotted against $[Ca^{2+}]_i$. Mean ± SEM (n = 7 to 14).

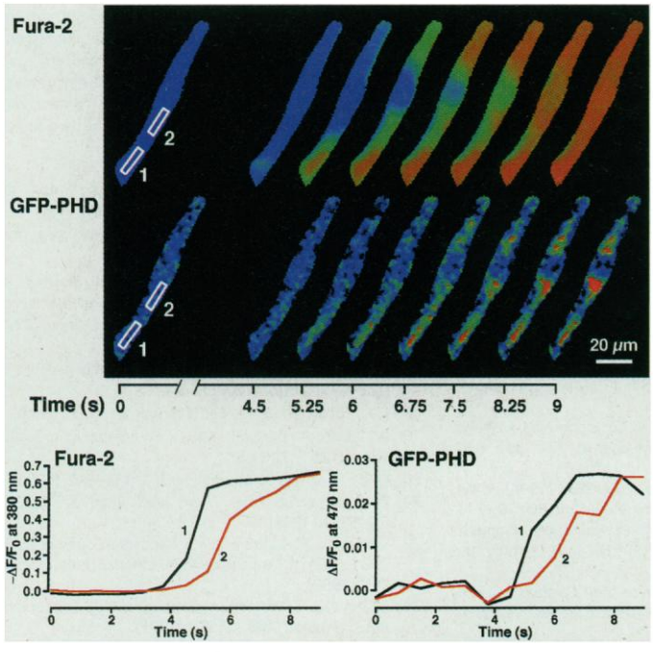

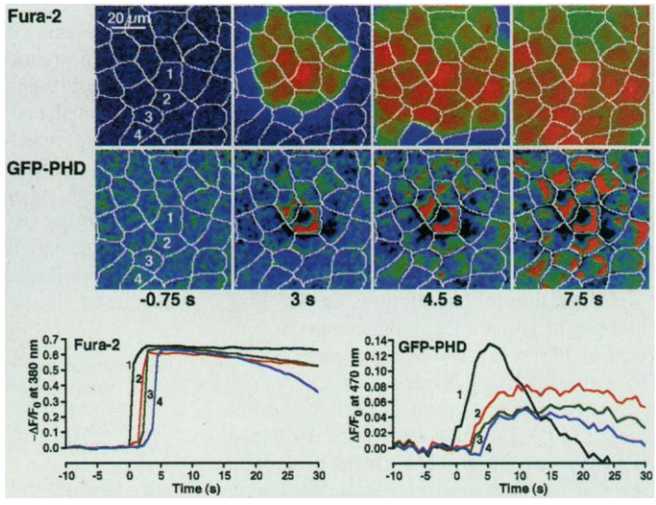

Fig. 4 (left). Intracellular dynamics of IP_3. Representative data from 16 cells that showed intracellular Ca^{2+} waves upon application of ATP (3 μM). The images normalized by the average of 10 images before stimulation are shown. The time courses of the signals from the regions, indicated by the numbered boxes, are plotted. Both Ca^{2+} and IP_3 waves start from the lower region of the cells. The upper region of the cell was another focus of the Ca^{2+} wave, which propagated downward until it reached the perinuclear region. Although the very early elevation of the IP_3 signal is difficult to see, the IP_3 wave is suggested by the delayed elevation in the perinuclear region. **Fig. 5 (right).** Mechanical stimulation of the cell numbered "1" with a fine glass capillary elicited an intercellular Ca^{2+} wave propagating to the neighboring cells. Ca^{2+} and IP_3 waves are monitored with fura-2 and GFP-PHD, respectively. The time courses of the signals are plotted for the cells numbered as indicated. Data shown are representative of four experiments.

tion in a dose-dependent manner resembling that by agonist stimulation (Fig. 2, C and D). U-73122, a PLC inhibitor (*15*), did not block this translocation (Fig. 2C), indicating that PIP_2 hydrolysis is not essential for this translocation. Nor was Ca^{2+} mobilization required, because depletion of the stores by ionomycin did not block the translocation (Fig. 2C). Because IP_3 5-phosphatase participates in the degradation of IP_3 (*16*), we examined the effect of its overexpression on GFP-PHD translocation. Translocation of GFP-PHD elicited by purinergic stimulation was abolished in the IP_3 5-phosphatase–expressing cells (Fig. 2E), indicating that an increase in $[IP_3]_i$ is necessary for the agonist-elicited translocation. Thus, an increase in $[IP_3]_i$ is both necessary and sufficient for the translocation of GFP-PHD. Moreover, complete abolition of the translocation by overexpression of IP_3 5-phosphatase indicates that during agonist stimulation, the concentration of free PIP_2 available to GFP-PHD remains either constant or greatly in excess of the K_d of PIP_2 binding (*17*).

We monitored the translocation of GFP-PHD to analyze changes in $[IP_3]_i$ associated with complex Ca^{2+} mobilization patterns. GFP-PHD–expressing cells were incubated with the Ca^{2+} indicator, fura-2. The negligible overlap in the excitation spectra of GFP and fura-2 enabled us to detect both Ca^{2+} and IP_3 signals simultaneously. ATP (1 to 3 μM) often elicited Ca^{2+} oscillations in MDCK cells (*18*), and oscillatory translocation of GFP-PHD synchronous with Ca^{2+} oscillations was observed (Fig. 3A). IP_3 oscillations have been suggested by measurement of $[IP_3]_i$ in a large population of cells in which Ca^{2+} oscillations were synchronized by removal and restoration of extracellular Ca^{2+} (*19*), although the validity of this technique has been challenged (*20*). Our results provide evidence for IP_3 oscillations accompanying Ca^{2+} oscillations at the single-cell level.

Generation of oscillations in $[IP_3]_i$ is thought to require Ca^{2+}-dependent activation of PLC (*19*, *21*). We therefore examined the effect of intracellular Ca^{2+} concentration ($[Ca^{2+}]_i$) on ATP-induced increase in $[IP_3]_i$. When cells were incubated with ionomycin or thapsigargin to deplete the Ca^{2+} stores and then stimulated with ATP, translocation of GFP-PHD was observed without any change in $[Ca^{2+}]_i$. A subsequent increase in the extracellular Ca^{2+} concentration induced Ca^{2+} influx, which then elicited further translocation (Fig. 3, B and C). However, the increase in $[IP_3]_i$ was transient and began to decrease, whereas the $[Ca^{2+}]_i$ continued to increase (Fig. 3B). The relation between $[Ca^{2+}]_i$ and translocation of GFP-PHD changed with time, and at higher $[Ca^{2+}]_i$, a pronounced time-dependent inhibition was observed (Fig. 3C). These results indicate that Ca^{2+} has both enhancing and inhibitory effects on $[IP_3]_i$ increase.

We analyzed spatial changes in $[IP_3]_i$ in detail during the early phase of the increase in $[Ca^{2+}]_i$ accompanying intracellular Ca^{2+} waves in MDCK cells after purinergic stimulation (Fig. 4). Translocation of GFP-PHD occurred concomitantly with Ca^{2+} wave propagation, indicating the presence of IP_3 waves. Taking into consideration the inherent kinetic and diffusional delay in the GFP-PHD signal, $[Ca^{2+}]_i$ and $[IP_3]_i$ waves appeared almost simultaneously, supporting the models in which regenerative Ca^{2+}-mediated IP_3 production accompanies Ca^{2+} waves or oscillations (*19*, *21*).

Mechanical stimulation of MDCK cells initiated intercellular Ca^{2+} waves that spread toward peripheral cells (Fig. 5) (*22*). Simultaneous imaging of GFP-PHD showed that the increase in $[IP_3]_i$ also spread in a wave pattern similar to that of the Ca^{2+} wave.

Our results provide insight into the mechanism of generation of complex Ca^{2+} signals. Two alternative mechanisms underlying the complex Ca^{2+} mobilization patterns have been proposed: Ca^{2+}-mediated positive and negative feedback mechanisms may control either the Ca^{2+} release process itself (mechanism 1) or IP_3 production (mechanism 2) (*1*, *3*, *4*). Our results are consistent with mechanism 2, which proposes the occurrence of oscillations in the $[IP_3]_i$ and IP_3 waves. We also observed Ca^{2+}-mediated enhancement and suppression of $[IP_3]_i$ increase, both of which are postulated in mechanism 2. However, our results do not exclude mechanism 1, and Ca^{2+}-mediated regenerative mechanisms of both Ca^{2+} release and IP_3 production may participate cooperatively in the generation of complex Ca^{2+} signaling patterns. Regarding the intercellular Ca^{2+} wave, intercellular diffusion of IP_3 may be also involved (*23*). The relative contribution of these mechanisms remains to be clarified.

References and Notes

1. M. J. Berridge, *Nature* **361**, 315 (1993); D. E. Clapham, *Cell* **80**, 259 (1995).
2. R. E. Dolmetsch, R. S. Lewis, C. C. Goodnow, J. I. Healy, *Nature* **386**, 855 (1997); W. Li *et al.*, *ibid.* **392**, 936 (1998).
3. M. J. Berridge, *J. Biol. Chem.* **265**, 9583 (1990); R. W. Tsien and R. Y. Tsien, *Annu. Rev. Cell Biol.* **6**, 715 (1990); T. Meyer and L. Stryer, *Annu. Rev. Biophys. Biophys. Chem.* **20**, 153 (1991); J. W. Putney Jr., *Science* **262**, 676 (1993).
4. T. A. Rooney and A. P. Thomas, *Cell Calcium* **14**, 674 (1993); H. Kasai and O. H. Petersen, *Trends. Neurosci.* **17**, 95 (1994).
5. A. Miyawaki *et al.*, *Nature* **388**, 882 (1997).
6. R. Y. Tsien and A. Miyawaki, *Science* **280**, 1954 (1998).
7. T. P. Stauffer, S. Ahn, T. Meyer, *Curr. Biol.* **8**, 343 (1998).
8. The cDNA encoding the PH domain of PLC-δ_1 (amino acid residues 11 to 140) was prepared with rat brain mRNA as a template by reverse transcriptase polymerase chain reaction (RT-PCR) based on the reported sequence [P. G. Suh *et al.*, *Cell* **54**, 161 (1988)]. pEGFP (Clontech) was used as a PCR template for GFP. The PCR products were subcloned into expression vectors to produce GFP-PHD in which the COOH-terminus of GFP and the NH_2-terminus of the PH domain were joined by a linker, Arg-Gly-Ser. The cDNA was subcloned into pET23a (Novagen) and expressed in *E. coli*, BL-21 (DE3). GFP-PHD was purified with an nitrilotriacetate-immobilized resin (Amersham-Pharmacia).
9. PIP_2 binding was examined with BIAcore equipped with a sensor chip HPA (Amersham-Pharmacia), onto which phosphatidycholine containing 0 or 3% PIP_2 was adsorbed. Specific binding was evaluated by the difference of resonance signals with and without PIP_2 on the sensor chip.
10. M. E. Cifuentes, T. Delaney, M. J. Rebecchi, *J. Biol. Chem.* **269**, 1945 (1994); H. Yagisawa *et al.*, *ibid.*, p. 20179; M. A. Lemmon, K. M. Ferguson, R. O'Brien, P. B. Sigler, J. Schlessinger, *Proc. Natl. Acad. Sci. U.S.A.* **92**, 10472 (1995).
11. The cDNA encoding GFP-PHD was cloned into pcDNA3.1 (Invitrogen) and introduced into MDCK cells (HSRB, Japan) by electroporation. The transfected cells were examined after 1 or 2 days. Stable transfectants were also established by G418 selection and cloning. The cytoplasmic concentrations of GFP-PHD were estimated to be 0.7 and 2 μM. No change in Ca^{2+} mobilization was found. The cDNA encoding rat IP_3 5-phosphatase was prepared by RT-PCR based on the reported sequences [K. M. Laxminarayan *et al.*, *J. Biol. Chem.* **269**, 17305 (1994); B. Verjans *et al.*, *Biochem. J.* **300**, 85 (1994)].
12. MDCK cells expressing GFP-PHD were grown on glass cover slips and were imaged with a confocal microscope (Fluoview, Olympus) with water (magnification, ×60; numerical aperture, 0.9) or oil (magnification, ×100; numerical aperture, 1.35) immersion objectives at 488-nm excitation. The cells were also imaged with a cooled charge-coupled device (CCD) camera (Photometrics) at 515 to 550 nm with excitation wavelengths of 340 (or 355) and 380 nm for fura-2 and 470 nm for GFP. For blue fluorescent protein (BFP) imaging, the excitation and emission wavelengths were 380 and 450 to 480 nm, respectively. GFP-PHD signal with the CCD camera was diluted because of the out-of-focus light by a factor of 5.9.
13. K. Hirose, unpublished data.
14. H. F. Paterson *et al.*, *Biochem. J.* **312**, 661 (1995); H. Yagisawa *et al.*, *J. Biol. Chem.* **273**, 417 (1998).
15. R. J. Smith *et al.*, *J. Pharmacol. Exp. Ther.* **253**, 688 (1990).
16. C. P. Downes, M. C. Mussat, R. H. Michell, *Biochem. J.* **203**, 169 (1982); P. W. Majerus, *Annu. Rev. Biochem.* **61**, 225 (1992); F. De Smedt *et al.*, *J. Biol. Chem.* **272**, 17367 (1997).
17. Absolute calibration of $[IP_3]_i$ is not possible because it requires quantification of free $[PIP_2]$.
18. J. A. Röttingen *et al.*, *Cell Calcium* **21**, 195 (1997).
19. A. T. Harootunian, J. P. Kao, S. Paranjape, R. Y. Tsien, *Science* **251**, 75 (1991).
20. M. D. Bootman *et al.*, *Biochem. J.* **314**, 347 (1996).
21. T. Meyer and L. Stryer, *Proc. Natl. Acad. Sci. U.S.A.* **85**, 5051 (1988).
22. S. Boitano, E. R. Dirksen, M. J. Sanderson, *Science* **258**, 292 (1992); Y. Osipchuk and M. Cahalan, *Nature* **359**, 241 (1992).
23. J. Sneyd, B. T. Wetton, A. C. Charles, M. J. Sanderson, *Am. J. Physiol.* **268**, C1537 (1995).

24. Supported in part by the Ministry of Education, Science, Sports and Culture of Japan. We thank M. Bougaki for his help in the construction of the GFP-PHD.

7 December 1998; accepted 21 April 1999